ACCORD flat-rate stay report

Stay: PH3: Clouds-precipitation microphysics, PH3.2: analysis of aerosols introduction to APLMPHYS
Author: David Nemec
Supervisor: Kwinten Van Weverberg
Location: Belgium
Date: from 2024-09-02 to 2024-09-20 (3 weeks)

Towards double-moment parameterization of rain

1 Introduction

The long-term goal regarding the microphysics parameterization in the ALARO model is to extend the current microphysics scheme in ALARO for a second moment, at least for selected hydrometeors, and make it sensitive to aerosol concentrations.

The current single-moment ALARO microphysics scheme has no term sensitive to the prescribed or prognostic aerosol concentration. Adding the second moment of the size distribution (number concentration) to the parameterization of cloud water allows for the straightforward use of aerosols as they act as cloud condensation nuclei. An activation scheme must be employed to obtain the number of activated aerosols, so the number concentration of cloud water. Once the mass fraction and number concentration of cloud water are estimated, rain can be created by further microphysical processes, firstly by autoconversion, which is for the double-moment cloud water sensitive to the number concentration.

The aim in the scope of the ALARO model is to make the double-moment scheme compatible with the moist deep convection parameterization 3MT ([GPB+09]), so implement all modifications to the sequence of routines computing various processes simulated by the 3MT scheme. However, all simulations in this report do not use 3MT as it simplifies the development of the new scheme.

The double-moment ALARO microphysics scheme is progresively developed. The status before the stay was such that the second moment of cloud water was already implemented, so the stay focused on the parameterization of double-moment rain, for which parameterization choices needed to be done and extensive tuning was necessary. This summary presents some options for parameterizing microphysical processes of the double-moment rain rather than a comprehensive overview of all tests of different tunings of all processes. Moreover, the scheme is only very briefly described as this text focuses on the developments from the stay, and details of the scheme are expected to change in the future. A more comprehensive documentation will be prepared once the scheme is further developed.

2 Double-moment microphysics in ALARO: current status

2.1 Scientific overview

Currently, only the number concentrations of cloud droplets and raindrops are prognostically computed. Both follow the gamma distribution:

$$N_x(D) = N_x \rho_a \frac{\lambda_x^{\mu_x+1}}{\Gamma(\mu_x+1)} D_x^{\mu_x} e^{-\lambda_x D_x}, \tag{1}$$

where $N_x(D)$ is the probability density function of number concentration, N_x is the total number concentration of the hydrometeor, ρ_a the air density, D is the diameter of the hydrometeor x, μ_x its shape parameter, and λ_x its slope parameter written as

$$\lambda_x = \left[\frac{\rho_x \pi N_x \Gamma(\mu_x+4)}{6\Gamma(\mu_x+1) q_x}\right]^{\frac{1}{3}}, \tag{2}$$

where ρ_x is the density of the hydrometer and q_x is its mass fraction.

The mass fraction of cloud water has two sources if 3MT is used: cloud scheme and updraft computed in 3MT. This is unchanged with the new scheme. The first change is that the activation of aerosols is computed. The activation scheme is the [FH92] one. The number of activated aerosols is based on the vertical velocity, temperature, and number concentration of aerosols. The self-collection of cloud droplets (collection of cloud water by cloud water) is computed following [Beh94] as a sink term of the cloud water number concentration. Once the number concentration is obtained, microphysical processes are sequentially computed, namely autoconversion, collection, self-collection/breakup of raindrops, evaporation, and melting. Formulae of all processes are, of course, rederived to account for the new size distribution.

The formulation of autoconversion and collection is discussed in Subsection 3.1. The parameterization of self-collection is discussed in Subsection 3.3. Finally, the parameterization of evaporation and melting stays as they are currently used in the operational setup at CHMI. For evaporation, the [Lop02] evaporation option is used. For melting, the only current option is the Kessler parameterization.

2.2 Technical implementation

All developments are based on `CY46t1.bf7` with local CHMI modifications and with the latest physics developments containing the Copernicus Atmosphere Monitoring Service (CAMS) aerosols assembled by Piotr Sekuła based on the contributions of many authors. Therefore, the CAMS aerosols are already present in `aplpar` and ready to be used in microphysics (`aplmphys`). For the first tests, the climatological aerosols are used.

Regarding the code changes to make aerosols available in `aplmphys`, a new routine, `acactiv`, is introduced to compute the activation of aerosols just before the call of `aplmphys`. If `L3MT`, then it is called from `aplpar`, if `LSTRAPRO=.T.`, then from `accdev`. Its output is the number concentration of cloud droplets, which enters `aplmphys`. To speed up the computation of activation, the values of activation are precomputed in the zeroth time-step in routine `arpifs/phys_dmn/suactiv.F90` called from `arpifs/phys_dmn/suphmf.F90` and stored in a look-up table.

3 Experiments

For all here presented simulations, the 3D version of the model is used, although the 1D version was extensively used for the first tests. The configuration uses the current operational model setup used at CHMI in September 2024, only without using the moist deep convection parameterization 3MT. The model horizontal resolution is 2.325 km (1069x853 points in the inner domain) with 87 levels. The time-step is 90 s. The reference configuration of microphysics is described in [NBVG24].

For presented tests, cases of strong convection on 2023-08-26 and 2022-06-24, and a typical autumn case with drizzle and also heavier precipittion on front on 2021-11-18 are used.

3.1 Autoconversion and collection

3.1.1 Theory

The current single-moment scheme uses the [Sun78] autoconversion parameterization, which can be written for rain as

$$\left(\frac{dq_l}{dt}\right)_{aco} = -k_r q_l \left\{1 - \exp\left[-\frac{\pi}{4}\left(\frac{q_l}{q_l^{crit}}\right)^2\right]\right\} \tag{3}$$

where q_l is the mass fraction of cloud water, q_l^{crit} its threshold value, and k_r is the autoconversion coefficient. The continuous collection model is used for collection.

As the current autoconversion parameterization is not sensitive to the cloud water number concentration, two other approaches are considered for the double-moment option. One is to use the parameterization proposed by [KK00] based on data from LES simulations of marine stratocumulus. The autoconversion from cloud droplets to raindrops is written as

$$\left(\frac{dq_l}{dt}\right)_{aco} = -1350 q_l^{2.47} (N_l \rho_a)^{-1.79}, \tag{4}$$

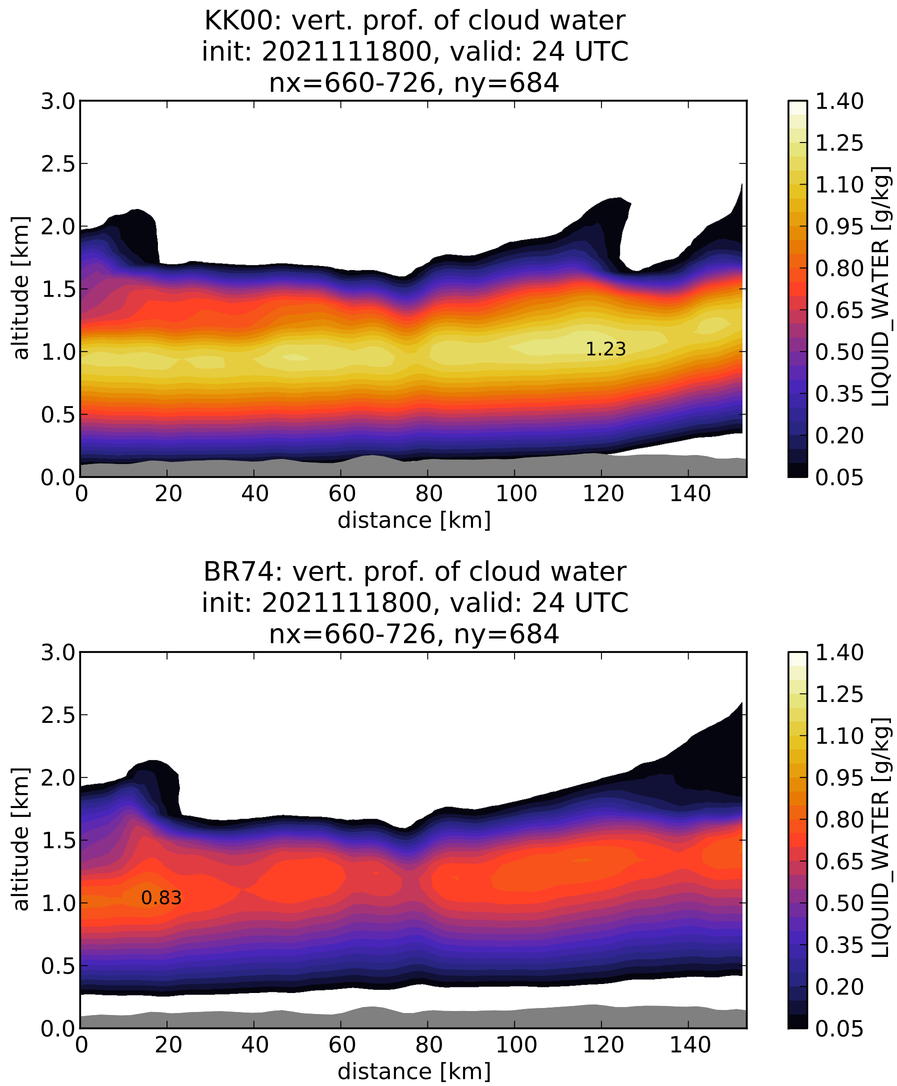

Figure 1: Vertical cross-section of q_l for an autumn case on 2021-11-18 near the shallow front. Upper: KK00 parameterization, lower: BR74 with continuous collection model.

where N_l [kg^{-1}] is the number concentration of cloud water, and ρ_a is the air density. A complementary collection parameterization is proposed as

$$\left(\frac{dq_l}{dt}\right)_{col} = -67(q_l q_r)^{1.15}, \tag{5}$$

where q_r is the mass fraction of rain.

The other tested option is the [BR74] autoconversion parameterization modified by [TFRH08], written as

$$\left(\frac{dq_l}{dt}\right)_{aco} = -7.25 \cdot 10^{-3} \rho_a^2 q_l^2 \left(6.25 \cdot 10^{18} D_b^3 \overline{D_l^V} - 0.4\right) \left(5 \cdot 10^5 D_b - 7.5\right), \tag{6}$$

where both brackets must be greater than 0 for autoconversion (no conversion back to cloud water) and

$$\overline{D_l^V} = \left(\frac{6q_l}{\pi \rho_w N_l}\right)^{\frac{1}{3}}, \qquad D_g = \frac{\left[\frac{\Gamma(\mu_l+7)}{\Gamma(\mu_l+4)}\right]^{\frac{1}{3}}}{\lambda_l}, \qquad D_b = \left(\overline{D_l^V}^3 D_g^3 - \overline{D_l^V}^6\right)^{\frac{1}{6}} \tag{7}$$

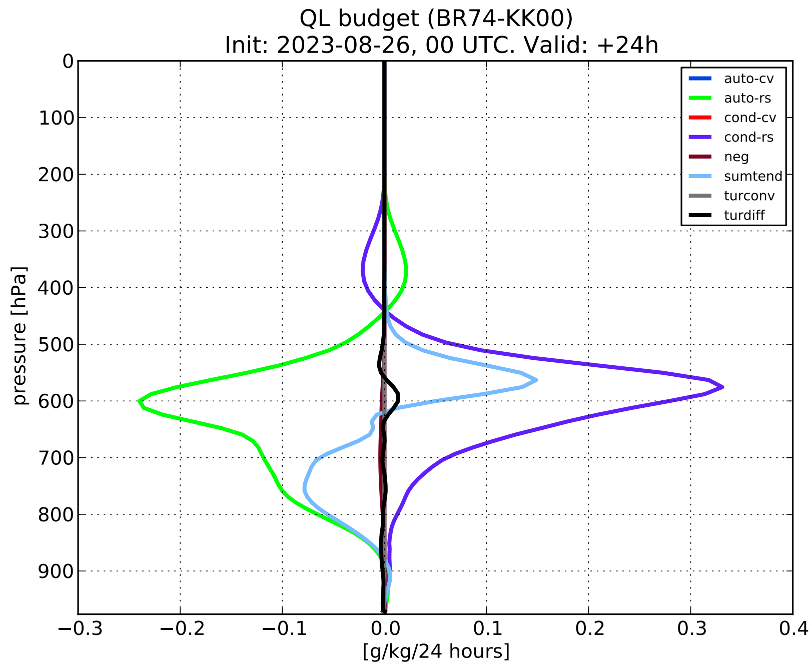

Figure 2: The DDH budget difference of q_l (BR74-KK00) for a summer convective case. The abbreviations are explained in Table 1.

where ρ_w is the density of water, and μ_l the shape parameter of the gamma size distribution for cloud water, and λ_l is given by Equation (2). This autoconversion is then used with the continuous collection model.

The autoconversion rates delivered by the [KK00] autoconversion are much lower compared to the [BR74] one, emphasizing the need for using the [KK00] collection parameterization with their autoconversion parameterization.

3.1.2 Results

There is quite a significant difference in the liquid water content delivered by these parameterizations if there is no precipitation in the solid phase. Thus, all rain is created from the so-called warm-rain processes. This is mainly apparent in autumn in cases with stratus and stratocumulus. Then, the KK00 parameterization delivers too thick clouds, in agreement with [WPB$^+$13].

Figure 1 shows a vertical cross-section of q_l on a shallow cold front on 2021-11-19 00 UTC. In this case, the melting level was just above the top of the cloud, so all precipitation was created by autoconversion from cloud water to rain. KK00 delivers much more q_l than BR74. Also, the cloud base is not elevated with KK00.

We can take a look at available observations for this case. Although the comparison will be very rough and far from any rigorous validation, it can provide some qualitative estimation of the results delivered by these two options. Also, although this figure shows a somewhat arbitrary example (more cross-sections were studied), the values of q_l and its maximum value stay similar in many cross-sections, which are not shown here. Compared to data from radiosondes from Lindenberg and Greifswald, the relative humidity of 100% was reached at 100-150 m above the ground, with the relative humidity near the ground around 95% for Lindenberg ([oW24b]) and 90% for Greifswald ([oW24a]), so the cloud base was likely lifted.

Data from a single-pointing radiometer from Warsaw ([JS24]) delivers estimates of the liquid water path, hovering around $0.4\,\mathrm{kg{\cdot}m^{-2}}$ before the rain started. The data from the radiosondes and the single-pointing radiometer seem to correspond with the expected behavior: the cloud is too thick with the KK00 scheme.

However, the cloud base height and liquid water content are not determined only by microphysics and macrophysics of clouds and precipitation, as turbulence plays a significant role, so there is always much feedback. Nonetheless, there is often a broad area of significant q_l in the lowest model level with the KK00

Table 1: List of abbreviations used for contributors in graphs in the DDH diagnostics.

abbreviation	**meaning**
auto-cv	convective autoconversion
auto-rs	resolved autoconversion
condcv or cond-cv	condensation in updraught
condrs or cond-rs	resolved condensation
dynam	dynamics
evapcv	evaporation in downdraft
evaprs	resolved evaporation
neg	correction for negative values
resid	residuals
(sum)tend	total tendency
turconv	vertical convective transport
turdiff	vertical turbulent transport

scheme in autumn, which does not seem to be observed. Therefore, the BR74 option seems to work better in autumn.

The difference in observed fields of q_l is smaller in convective cases as the precipitation onset is not controlled by autoconversion from cloud water to rain since there is interaction with solid phase hydrometeors. There is bigger difference due to different collection parameterizations, which modifies the contribution to the DDH budget, although the resulting precipitation fields seem similar (not shown). Figure 2 shows the q_l budget difference between BR74 (experiment) and KK00 (reference). There is an apparent increase in autoconversion and collection with BR74 (autoconversion and collection are grouped together to `auto-rs`). Consequently, condensation (`cond-rs`) is less as less condensed water is carried out to the surface by rain. There is also less cloud water below the melting level (around 650 hPa) due to different combinations of autoconversion and collection parameterization. This is often tuned in the continuous collection model by the value of collection efficiency, which was, in this case, equal to 1. Its value might be reassessed in the future.

3.2 Excessive size-sorting

3.2.1 Theory

A common flaw of double-moment microphysics schemes is too strong size sorting implied by different fall speeds of the two moments when the fall speed of mass is always faster than that of number, which can be easily proven. One starts from the general prescription of the dependency of fall speed on the diameter of the drop, which is in ALARO:

$$w(D) = a_0 D^{\alpha} \left(\frac{\rho_0}{\rho}\right)^{\alpha}, \tag{8}$$

where $a_0 = 654.5\,\mathrm{m}^{0.2294}\mathrm{s}^{-1}$ and $\alpha = 0.7706$ are coefficients, ρ_0 is the reference air density, and D is the diameter of the drop. As raindrops are assumed to be spherical, their mass is

$$m(D) = \frac{\pi D^3}{6}\rho_w. \tag{9}$$

One can finally proceed to the computation of the mass-weighted fall speed:

$$w_m = \frac{\int\limits_0^\infty w(D)m(D)N(D)dD}{\int\limits_0^\infty m(D)N(D)dD} = a_0\left(\frac{\rho_0}{\rho_a}\right)^{\alpha} \frac{\int\limits_0^\infty D^{3+\alpha+\mu_r}e^{-\lambda D}}{\int\limits_0^\infty D^{3+\mu_r}e^{-\lambda D}} = a_0\left(\frac{\rho_0}{\rho_a}\right)^{\alpha} \frac{\Gamma\left(4+\mu_r+\alpha\right)}{\Gamma\left(4+\mu_r\right)}\frac{\lambda^{4+\mu_r}}{\lambda^{4+\alpha+\mu_r}}, \tag{10}$$

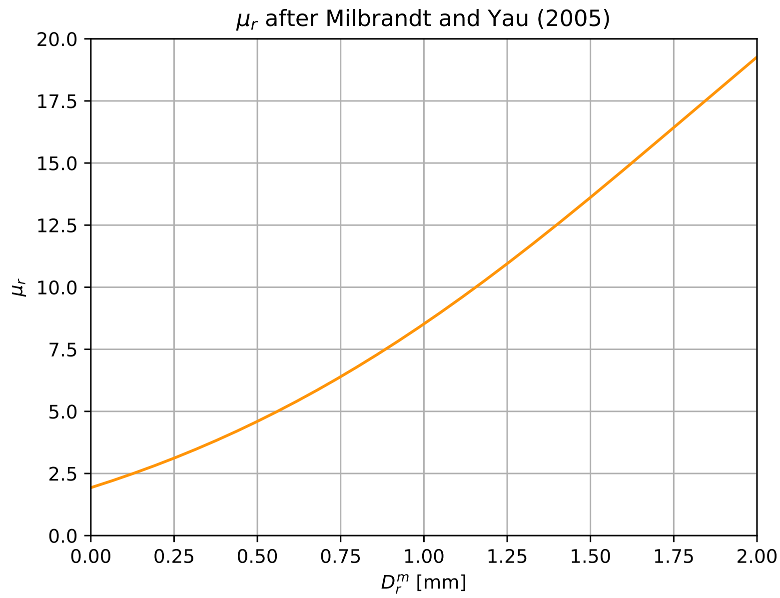

Figure 3: The shape of diagnostic function for μ_r following [MY05].

and the number-weighted fall speed:

$$w_N = \frac{\int_0^\infty w(D)N(D)dD}{\int_0^\infty N(D)dD} = a_0\left(\frac{\rho_0}{\rho_a}\right)^\alpha \frac{\int_0^\infty D^{\alpha+\mu_r}e^{-\lambda D}}{\int_0^\infty D^{\mu_r}e^{-\lambda D}} = a_0\left(\frac{\rho_0}{\rho_a}\right)^\alpha \frac{\Gamma\left(1+\mu_r+\alpha\right)}{\Gamma\left(1+\mu_r\right)}\frac{\lambda^{1+\mu_r}}{\lambda^{1+\alpha+\mu_r}}. \tag{11}$$

Their ratio is then

$$\frac{w_m}{w_N} = \frac{\Gamma\left(4+\mu_r+\alpha\right)}{\Gamma\left(4+\mu_r\right)}\frac{\Gamma\left(1+\mu_r\right)}{\Gamma\left(1+\mu_r+\alpha\right)} = \frac{\left(4+\mu_r+\alpha\right)\left(3+\mu_r+\alpha\right)\left(2+\mu_r+\alpha\right)}{\left(4+\mu_r\right)\left(3+\mu_r\right)\left(2+\mu_r\right)} \geq 1, \tag{12}$$

knowing that $\mu_r, \alpha \geq 0$. Alternatively, we get that term $\frac{\Gamma(4+\mu_r+\alpha)}{\Gamma(4+\mu_r)}$ must be greater than $\frac{\Gamma(1+\mu_r+\alpha)}{\Gamma(1+\mu_r)}$ using the Jensen's inequality.

Apparently, raising the value of μ_r might be one option for reducing the excessive size sorting. Indeed, [MY05] proposed one such option:

$$\mu_r = c_{1r}\tanh\left[c_{2r}\left(\overline{D_r^m} - c_{3r}\right)\right] + c_{4r}, \tag{13}$$

where D_r^m is the mass-weighted diameter in milimeters and $c_{1r} = 19.0$, $c_{2r} = 0.6\,\mathrm{mm}^{-1}$, $c_{3r} = 1.8\,\mathrm{mm}$, $c_{4r} = 17$ are constants. The shape of the function is shown in Figure 3. This function will be tested and compared to a fixed value of $\mu_r = 1$.

3.2.2 Results

Figure 4 shows the DDH budget difference of temperature and water vapor, where the experiment with $\mu_r = 1$ is the reference for the experiment with variable μ_r. The water vapor budget shows that there is much stronger evaporation with the variable shape parameter. Also the precipiatation field is broader with more light accumulations with the fixed parameter due to weaker evaporation (not shown).

The mean volume diameter $\overline{D_r^V}$ in the lowest model level is shown in the Figure 5. The variable shape parameter seems to slightly improve the problem of the excessive size sorting near the leading edge of the convective system, where drops reach the maximum allowed mean volume diameter of 1.7 mm. Also, the values of $\overline{D_r^V}$ are slightly reduced in the trailing stratiform region.

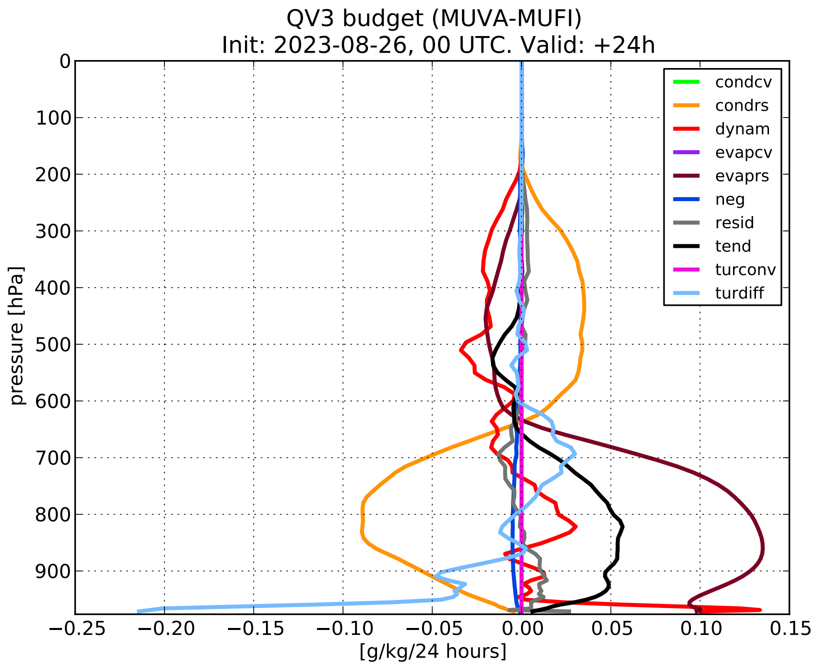

Figure 4: The DDH water vapor budget difference of an experiment with the variable shape paramter to an experiment with $\mu_r = 1$. The symbols are explained in Table 1.

Figure 6 shows the simulated reflectivities at approximately 2 km above the ground. It seems that the reflectivities are underestimated with the variable μ_r. On the other hand, the experiment with $\mu_r = 1$ delivers a more realistic reflectivity field compared to observations (not shown), although one must be careful with high reflectivities as hail and graupel are expected to change the measured reflectivities as there was frequent hail with diameters over 2 cm reported along the trajectory of this convective storm ([Eur23]).

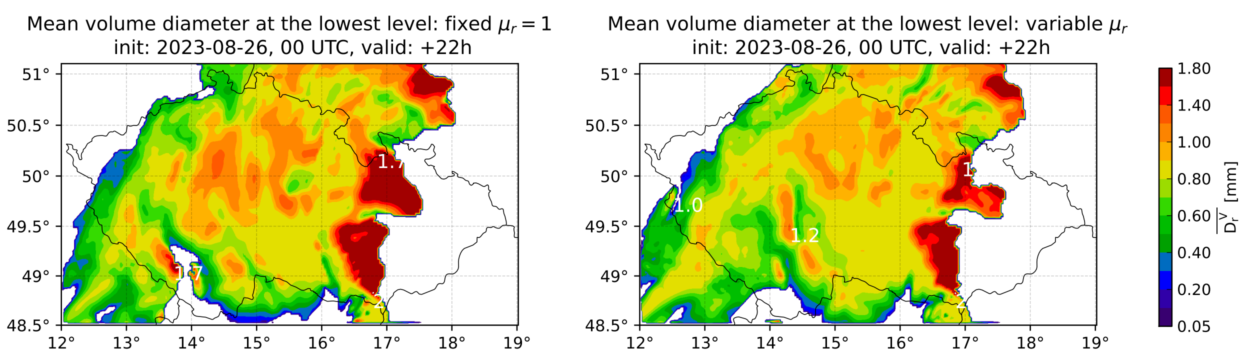

Figure 5: Mean volume diameter in the lowest model level with the fixed $\mu_r = 1$ (left) and the variable shape paramter (right).

3.3 Self-collection and breakup or raindrops

3.3.1 Theory

Self-collection describes the collection of particles in one category. That means that its number is changed, unlike its mass. Breakup is the opposite process when one drop breaks into two or more others. In the

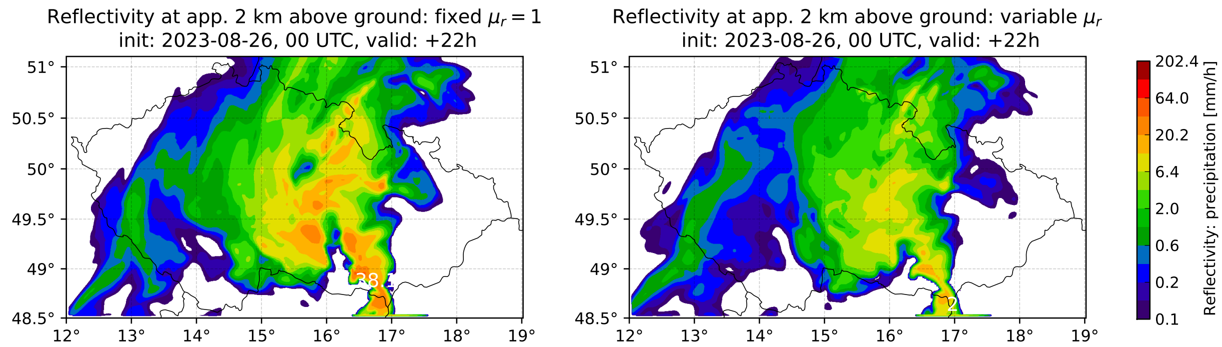

Figure 6: Simulated radar reflectivity at approximately 2 km above the ground for the experiment with fixed $\mu_r = 1$ (left) and the variable shape paramter (right). The field is recomputed using a Z-R relation with the standard coefficients $Z = 200R^{1.6}$, where Z is the reflectivity factor and R the precipitation rate.

currently used double-moment schemes, only collisional self-collection/breakup is parameterized, while spontaneous breakup is neglected, but often treated by limiting the maximum allowed diameter. In our case, the maximum allowed mean volume diameter is 1.7 mm.

For the tests, the approach of [Beh94] for collisional self-collection is employed:

$$\left(\frac{dN_r}{dt}\right)_{sc} = 8E_{rr}N_r q_r \rho_a, \tag{14}$$

where $E_{rr} < 0$ is the self-collection efficiency. This equation is also widely used for the breakup of drops by setting $E_{rr} > 0$ when drops become larger. For this study, we focus on the [VC93] parameterization of self-collection and breakup efficiency, written as

$$\begin{aligned} E_{rr} &= -1 & \overline{D_r^V} &< D_m = 6 \cdot 10^{-4}\, m \\ E_{rr} &= e^{2300(\overline{D_r^V} - D_m)} - 2 & \overline{D_r^V} &> D_m = 6 \cdot 10^{-4}\, m, \end{aligned} \tag{15}$$

where $\overline{D_r^V}$ is the mean volume diameter of rain and D_m is an arbitrary threshold, of which value can be tuned (some options were tested but they are not shown here) to find an optimal equlibrium diameter (for example using data from distrometers).

It is easy to see that the breakup efficiency for bigger $\overline{D_r^V}$ becomes very high. This was examined by [SDB+22], who found a "spike" around the equilibrium diameter of significantly increased frequency of such drop diameters. This was attributed to too high breakup efficiency forcing drops to have the size of the equlibrium diameter. Similar behavior was reported by [VWGB+14]. To avoid this, [VWGG+24] proposed to set a maximum $E_{rr,max} = 0.5$, based on the findings of [SDB+22]. Several thresholds are tested in the following part.

3.3.2 Results

For these tests, the variable shape parameter following Equation (13) was used. The aim is to reproduce Figure 1 from [SDB+22] for four maximum values of the break-up efficiency $E_{rr,max} = [0, 0.1, 0.5, 1]$. Figure 7 reproduces this figure for data from the lowest model level from the whole domain from a simulation on 2023-08-26, which was dominated by precipitation from convective storms. The spike reported by [SDB+22] is indeed present for $E_{rr,max} = 1$. However, the spike is present even with $E_{rr,max} = 0.5$ and also with $E_{rr,max} = 0.1$, although a little bit less pronounced.

There is also an influence of the shape parameter of rain, μ_r, as shown in the lowermost plot in Figure 7, which shows results from a simulation with $\mu_r = 1$ and $E_{rr,max} = 0.1$ (experiment MUBR is the same as MUFI in Subsection 3.2 and can be compared with SC01, because they differs only in the shape parameter of rain). The spike is slightly less pronounced with $\mu_r = 1$ and the distribution is broader towards larger diameters. However, the spike is still present and finding all reasons will require further analysis.

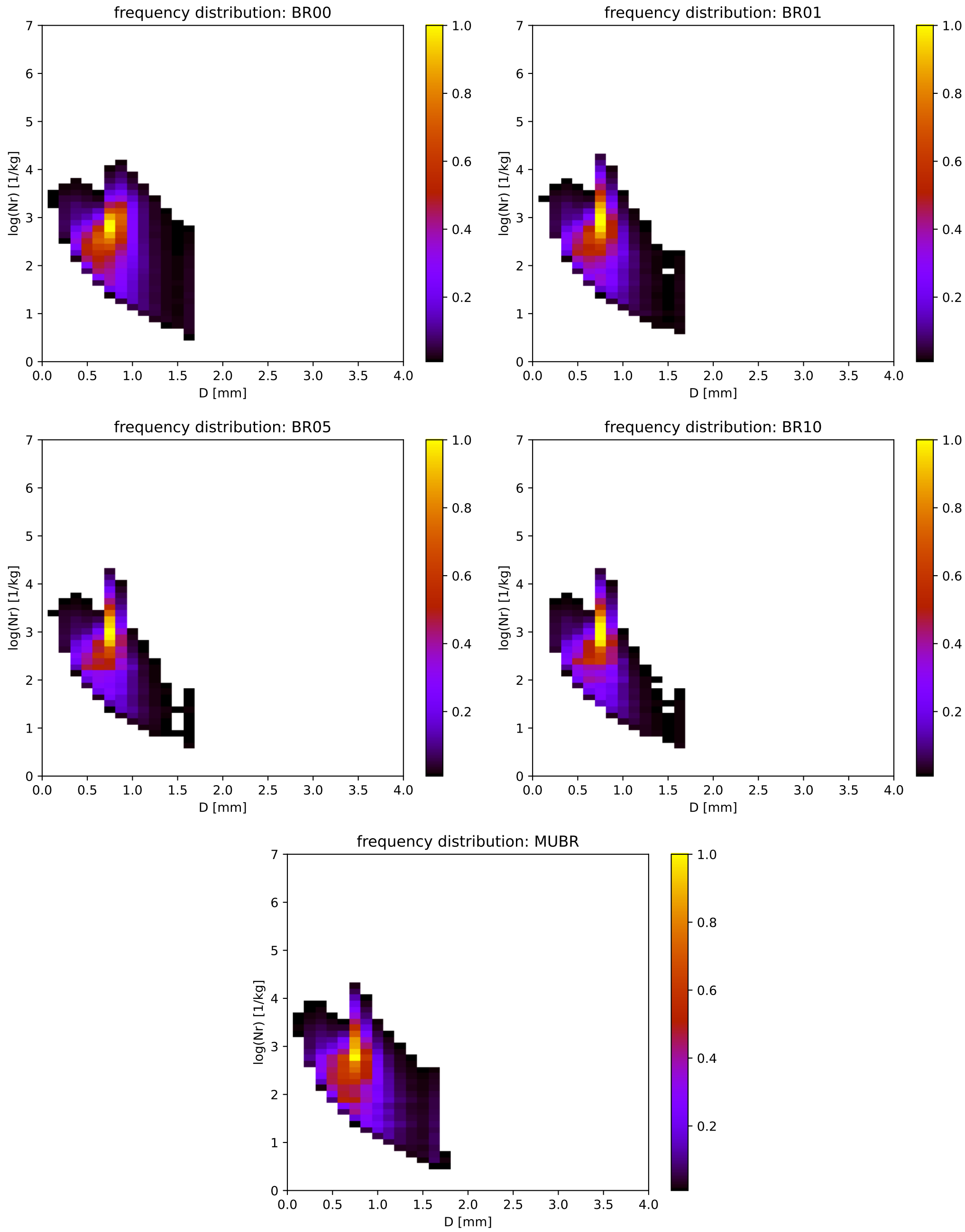

Figure 7: . Mean diameter frequency distribution with $\log N_r$ on hte vertical axis and $\overline{D_r^V}$ on horizontal, which replicates Figure 1 from [SDB+22] for various values of Err, max. Top left: $E_{rr,max} = 0$ (no break-up), top left: $E_{rr,max} = 0.1$, middle left: $E_{rr,max} = 0.5$, middle right $E_{rr,max} = 1$, bottom: $E_{rr,max} = 0.1$ with fixed $\mu_r = 1$. Experiments MUBR=MUFI and BR01=MUVA in the previous subsection.

Nonetheless, the value of $E_{rr,max} = 0.1$ is used for further tests as a full omitting of the process is not currently desired. There is also apparent that the maximum allowed mean volume diameter (1.7 mm) occurs quite frequently. A more in-depth validation against disdrometer data will be done later.

Generally, there is only a little difference in the precipitation fields and the DDH budgets (not shown) with the tested values of $E_{rr,max}$. A slight increase in evaporation is found with higher values of $E_{rr,max}$ due to smaller drops. Consequently, the precipitation accumulations near storms' edges are a little bit higher

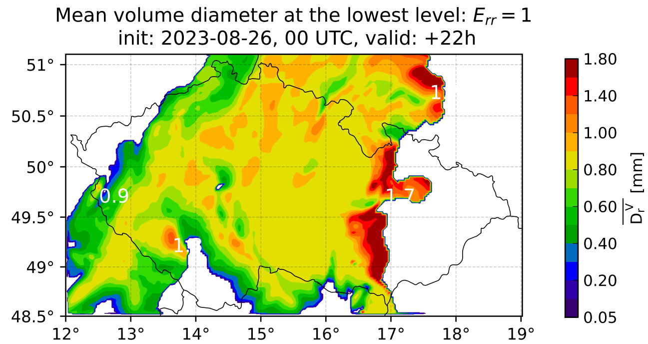

Figure 8: Mean volume diameter in the lowest level for the experiment with variable μ_r and $E_{rr,max} = 1$.

with lower values of $E_{rr,max}$, making the edges of precipitation a little bit smoother.

Figure 8 shows the mean volume diameter in the lowest level for the experiment with $E_{rr,max} = 1$. The more effective breakup helps to reduce the mean volume diameter at the leading edge of the storm (cf. Figure 5).

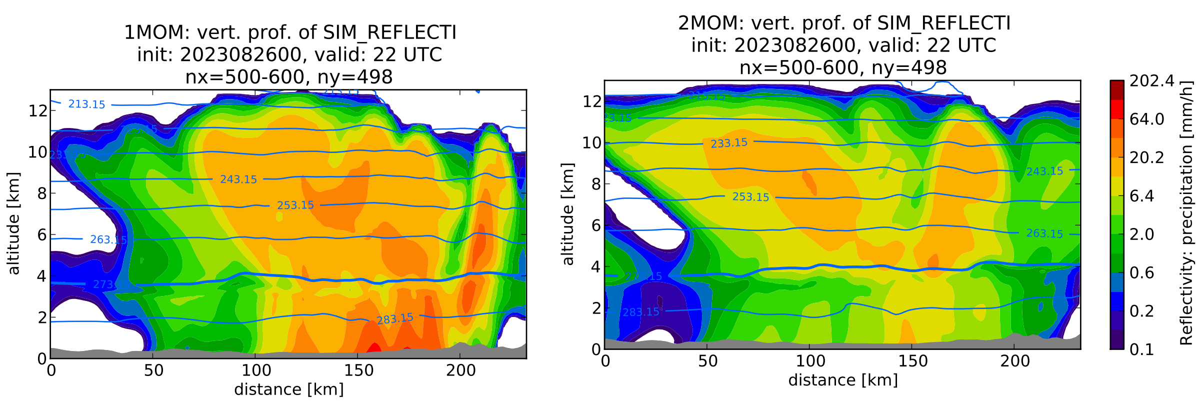

Figure 9: Vertical cross-section of simulated radar reflectivities (filled) and temperature (blue contours) of a mesoscale convective system. The case shown is from 2023-08-26 at 22 UTC created from the 3D model output near the 50N latitude, where the storm had high maximum reflectivity in both cases. The field is recomputed using a Z-R relation with the standard coefficients $Z = 200R^{1.6}$, where Z is the reflectivity factor and R the precipitation rate. Left: single-moment scheme with the Abel-Boutle rain distribution, right: scheme with double-moment cloud water and rain with variable μ_r. Note the apparent drop of radar reflectivity just below the melting level with the single-moment scheme.

4 Comparison to the single-moment scheme

For the comparison, 3MT is not used. The single-moment scheme version (1MOM) is identical to the operationally used in September 2024; only 3MT is switched off. The size distribution for rain is the Abel and Boutle one.

The double-moment version (2MOM) uses BR74 autoconversion with the continuous collection model (collection efficiencies of rain collecting cloud water and cloud ice are $E_{rl} = E_{ri} = 1$), initial diameter from autoconversion $d_{r,0} = 5 \cdot 10^{-5}$ m, break-up efficiency limited to $E_{rr} < 0.1$, variable μ_r following Equation (13), $\mu_l = 2$, and the minimal number concentration of cloud droplets $N_{l,min} = 3 \cdot 10^{-7}\,\text{kg}^{-1}$, which is a value tuned on various idealized cases on the single column model. The idealized cases are DYCOMS2 RF1 ([SMA+05]), DYCOMS2 RF2 ([ASSJ+09]) and ARMCU ([BCC+02]). The maximum allowed mean volume diameter of raindrops is 1.7 mm.

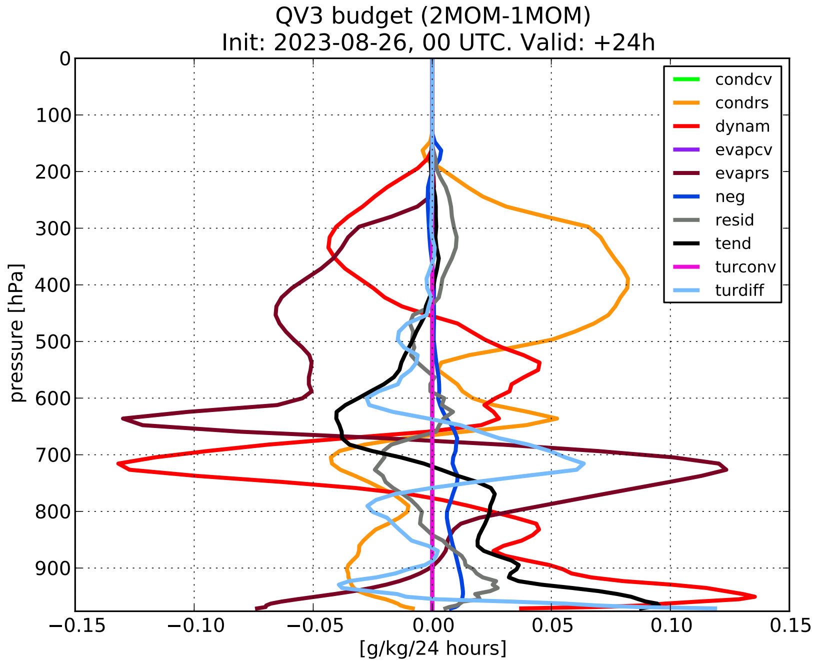

Figure 10: Water vapor budget difference between the double-moment scheme and single-moment scheme. The abbreviations are explained in Table 1. Note the reduction of evaporation near the melting layer around 650 hPa.

4.1 Size distributions

Currently, the single-moment scheme uses the [AB12] size distribution, which delivers very small drops if q_r is small. However, melting ice particles often produce big drops instead. This deficiency is observed in the vertical cross-sections of simulated radar reflectivities of convective storms. One such example is in Figure 9. There is an apparent drop of radar reflectivities just below the melting level, but the reflectivity quickly rises again, which might be called a reflectivity valley. This is caused by locally low q_r when snow and graupel are only partially melted. Due to small drop diameters at small q_r, the contribution of rain to the resulting reflectivity is underestimated. It must be noted that the reflectivity of graupel and snow uses size distributions from the ICE3 scheme, so the more important thing is the increase of reflectivity from rain towards lower levels.

Although less pronounced than in the single-moment version, there is still an apparent reflectivity “valley” in the double-moment version, maybe because of high fall speeds for big drops near the melting level. On the other hand, the reflectivity does not rise too much towards lower levels as in the single-moment version.

Figure 10 shows the water vapor budget difference for a summer case with severe convective storms. Due to larger drops delivered by the double-moment version, evaporation is quite abruptly reduced around 650 hPa. On the contrary, an increase of evaporation is found around 750 hPa due to the high amount of precipitation reaching these layers due to weaker evaporation right below the melting level.

4.2 Drizzle case

ALARO generally suffers from a positive precipitation bias in autumn. Especially, the area of low precipitation rates is overestimated ([NBVG24]). Figure 11 shows that with the double-moment scheme, light precipitation is reduced, mainly over Germany and the Netherlands. This is in contrast to the results with CASIM in the

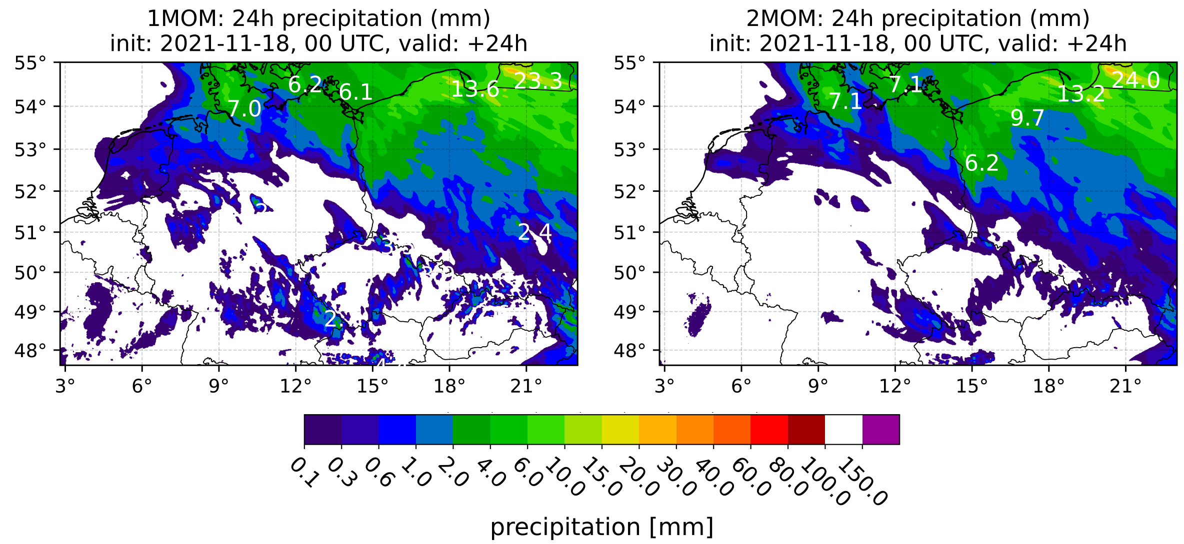

Figure 11: Comparison of the 24-hour precipitation accumulation ending on 2021-11-19 at 00 UTC. Top: single-moment rain and cloud water, bottom: double-moment rain and cloud water.

Unified Model ([FHS+23]). On the other hand, the heavier rain in the northeast of the shown domain is almost intact.

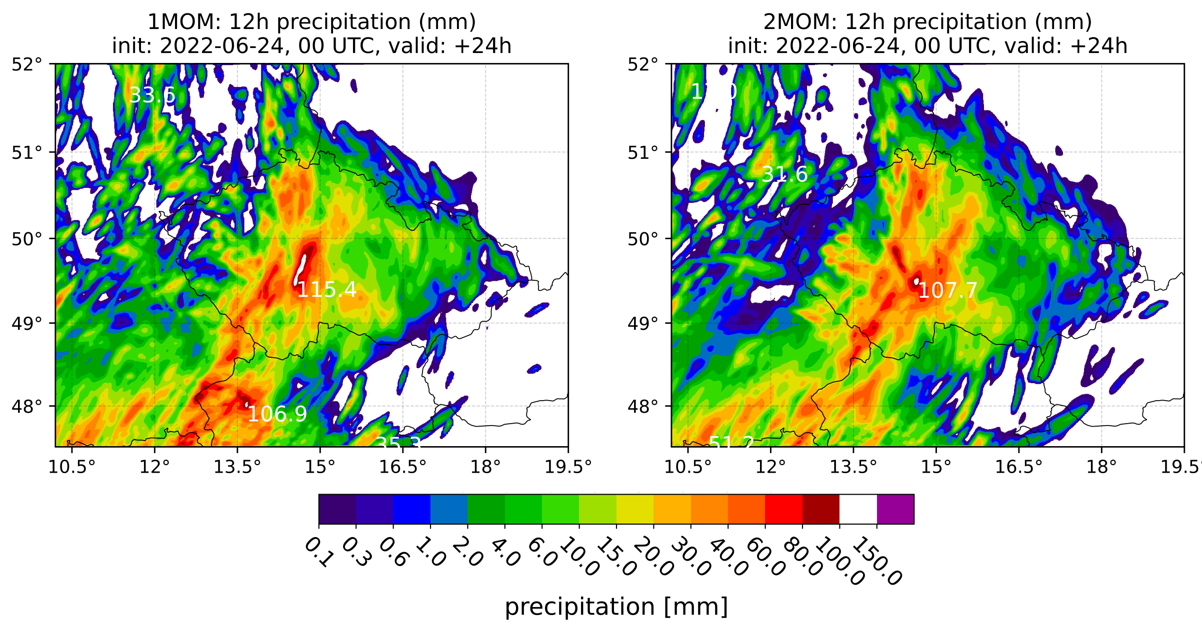

Figure 12: Comparison of the 12-hour precipitation accumulation ending on 2022-06-24 at 00 UTC. Top: single-moment rain and cloud water, bottom: double-moment rain and cloud water.

The reduction of light precipitation is caused mainly by less effective autoconversion. The minimum value of cloud droplet concentration $N_{l,min} = 3 \cdot 10^{-7}\,\mathrm{kg}^{-1}$. Generally, the higher the minimum value of cloud droplet concentration (here $N_{l,min} = 3 \cdot 10^{-7}\,\mathrm{kg}^{-1}$), the less light precipitation from low-level stratus as droplets are smaller and consequently less likely converted to raindrops. On the contrary, light precipitation from clouds with higher bases can be enhanced with the double-moment parameterization of rain, mainly if melting occurs below the cloud base (not shown).

4.3 Convective case

As opposed to the positive precipitation bias for light rain in the case of drizzle, light precipitation accumulations from convective storms are often underestimated by the ALARO single-moment scheme [NBVG24]. The main cause is too strong evaporation due to the prescribed size distribution. As mentioned in Subsection 4.1, the fixed distribution delivers small drops for small q_r. However, convective storms often produce big drops created by melting ice particles. This inconsistency leads to evaporation fluxes that are too high in the single-moment scheme, so less precipitation reaches the ground. This is improved with the double-moment scheme, but the drops are often too big due to the excessive size sorting, as mentioned in Subsection 3.2. The sizes of melting particles can be further enhanced by a correct double-moment representation of ice precipitating particles.

Figure 12 compares the precipitation delivered by the two versions of the microphysics scheme for a slowly moving mesoscale convective system on 2022-06-24. There is an apparent increase of light precipitation, mainly over Germany. The spread of heavy precipitation is slightly higher. The maximum value of the precipitation accumulation is similar, although slightly lower with the double-moment scheme. The slight reduction of precipitation maxima is often observed in other convective cases as well. It is likely connected to evaporation, as evaporation in heavy precipitation is usually higher with the double-moment scheme.

5 Conclusion and outlooks

During this stay, several options for parameterizing the double-moment rain were tested. Only basic validation was done because the objective was to compare selected options for parameterizing some microphysical processes and assess whether the new scheme has the potential to improve the results of the current single-moment scheme. Once the scheme is further developed, much more detailed validation is planned.

While we can see indications of improvement compared to the signle-moment scheme, the parameterization still needs to be tuned. In particular, the rain shape parameter will require furhter tuning. Data from disdrometers and comparing reflectivities more rigorously might help finding a better shape parameter.

The development of the double-moment scheme is expected to continue progressively, starting with tuning the double-moment rain to a physically and computationally satisfactory shape. Once the double-moment parameterization of the liquid phase is ready, the work will continue with an analysis of the usefulness and sustainability of a double-moment parameterization of the solid phase.

Acknowledgement

The author would like to thank Kwinten Van Weverberg for hosting me, all his support, valuable discussions, and reviewing this report. The author thanks ACCORD for funding this stay.

References

[AB12] S. J. Abel and I. A. Boutle. An improved representation of the raindrop size distribution for single-moment microphysics schemes. *Quarterly Journal of the Royal Meteorological Society*, 138(669):2151–2162, 2012.

[ASSJ+09] Andrew S Ackerman, Bjorn Stevens, Verica Savic-Jovcic, Christopher S Bretherton, Andreas Chlond, Jean-Christophe Golaz, Hongli Jiang, Marat Khairoutdinov, Steven K Krueger, David C Lewellen, et al. Large-eddy simulations of a drizzling, stratocumulus-topped marine boundary layer. *Monthly Weather Review*, 137(3):1083–1110, 2009.

[BCC+02] AR Brown, Richard T Cederwall, Andreas Chlond, Peter G Duynkerke, J-C Golaz, Marat Khairoutdinov, DC Lewellen, AP Lock, MK MacVean, C-H Moeng, et al. Large-eddy simulation of the diurnal cycle of shallow cumulus convection over land. *Quarterly Journal of the Royal*

Meteorological Society: A journal of the atmospheric sciences, applied meteorology and physical oceanography, 128(582):1075–1093, 2002.

[Beh94] KD Beheng. A parameterization of warm cloud microphysical conversion processes. *Atmospheric Research*, 33(1-4):193–206, 1994.

[BR74] E. X. Berry and R. L. Reinhardt. An analysis of cloud drop growth by collection part ii. single initial distributions. *Journal of Atmospheric Sciences*, 31(7):1825 – 1831, 1974.

[Eur23] European Severe Storms Laboratory. Large hail occurring between 26-8-2023 00:00:00 and 26-8-2023 24:00:00 GMT/UTC, 2023.

[FH92] Graham Feingold and Andrew J Heymsfield. Parameterizations of condensational growth of droplets for use in general circulation models. *Journal of the atmospheric sciences*, 49(23):2325–2342, 1992.

[FHS+23] Paul R Field, Adrian Hill, Ben Shipway, Kalli Furtado, Jonathan Wilkinson, Annette Miltenberger, Hamish Gordon, Daniel P Grosvenor, Robin Stevens, and Kwinten Van Weverberg. Implementation of a double moment cloud microphysics scheme in the uk met office regional numerical weather prediction model. *Quarterly Journal of the Royal Meteorological Society*, 149(752):703–739, 2023.

[GPB+09] L. Gerard, J.-M. Piriou, R. Brožková, Geleyn J.-F., and D. Banciu. Cloud and Precipitation Parameterization in a Meso-Gamma-Scale Operational Weather Prediction Model. *Monthly Weather Review*, 137(11):3960 – 3977, 2009.

[JS24] Łucja Janicka and Iwona Stachlewska. Mwr single pointing data from Warsaw on 18 and 19 November 2021, 2024. Data is volatile and may be updated in the future.

[KK00] M. Khairoutdinov and Y. Kogan. A New Cloud Physics Parameterization in a Large-Eddy Simulation Model of Marine Stratocumulus. *Monthly Weather Review*, 128(1):229 – 243, 2000.

[Lop02] Philippe Lopez. Implementation and validation of a new prognostic large-scale cloud and precipitation scheme for climate and data-assimilation purposes. *Quarterly Journal of the Royal Meteorological Society*, 128(579):229–257, 2002.

[MY05] J. A. Milbrandt and M. K. Yau. A Multimoment Bulk Microphysics Parameterization. Part I: Analysis of the Role of the Spectral Shape Parameter. *Journal of the Atmospheric Sciences*, 62(9):3051 – 3064, 2005.

[NBVG24] David Nemec, Radmila Brožková, and Michiel Van Ginderachter. Developments of single-moment alaro microphysics scheme with three prognostic ice categories. *Tellus A: Dynamic Meteorology and Oceanography*, 76(1), 2024.

[oW24a] University of Wyoming. Observations for Station 10184 starting 2244Z 18 Nov 2021, Greifswald, Germany, 2024.

[oW24b] University of Wyoming. Observations for Station 10393 starting 2245Z 18 Nov 2021, Lindenberg, Germany, 2024.

[SDB+22] Stephen M Saleeby, Brenda Dolan, Jennie Bukowski, Kristen Van Valkenburg, Susan C van den Heever, and Steven A Rutledge. Assessing raindrop breakup parameterizations using disdrometer observations. *Journal of the Atmospheric Sciences*, 79(11):2949–2963, 2022.

[SMA+05] Bjorn Stevens, Chin-Hoh Moeng, Andrew S Ackerman, Christopher S Bretherton, Andreas Chlond, Stephan de Roode, James Edwards, Jean-Christophe Golaz, Hongli Jiang, Marat Khairoutdinov, et al. Evaluation of large-eddy simulations via observations of nocturnal marine stratocumulus. *Monthly weather review*, 133(6):1443–1462, 2005.

[Sun78] Hilding Sundqvist. A parameterization scheme for non-convective condensation including prediction of cloud water content. *Quarterly Journal of the Royal Meteorological Society*, 104(441):677–690, 1978.

[TFRH08] G. Thompson, P. R. Field, R. M. Rasmussen, and W. D. Hall. Explicit Forecasts of Winter Precipitation Using an Improved Bulk Microphysics Scheme. Part II: Implementation of a New Snow Parameterization. *Monthly Weather Review*, 136(12):5095 – 5115, 2008.

[VC93] Johannes Verlinde and William R Cotton. Fitting microphysical observations of nonsteady convective clouds to a numerical model: An application of the adjoint technique of data assimilation to a kinematic model. *Monthly weather review*, 121(10):2776–2793, 1993.

[VWGB+14] Kwinten Van Weverberg, Edouard Goudenhoofdt, Ulrich Blahak, Erwan Brisson, Matthias Demuzere, Philippe Marbaix, and Jean-Pascal van Ypersele. Comparison of one-moment and two-moment bulk microphysics for high-resolution climate simulations of intense precipitation. *Atmospheric research*, 147:145–161, 2014.

[VWGG+24] Kwinten Van Weverberg, Nicolas Ghilain, Edouard Goudenhoofdt, Matthias Barbier, E Koistinen, Sébastien Doutreloup, Bert Van Schaeybroeck, Amaury Frankl, and Paul Field. Sensitivity of simulated rain intensity and kinetic energy to aerosols and warm-rain microphysics during the extreme event of July 2021 in Belgium. *Quarterly Journal of the Royal Meteorological Society*, 2024.

[WPB+13] J. M. Wilkinson, A. N. F. Porson, F. J. Bornemann, M. Weeks, P. R. Field, and A. P. Lock. Improved microphysical parametrization of drizzle and fog for operational forecasting using the Met Office Unified Model. *Quarterly Journal of the Royal Meteorological Society*, 139(671):488–500, 2013.